THE JOURNAL OF PHYSICAL CHEMISTRY C

Subscriber access provided by BUFFALO STATE

C: Surfaces, Interfaces, Porous Materials, and Catalysis

Mechanistic Insight Into Gas Cluster-Induced Sputtering of Kilodalton Molecules Using Kinetic Energy Distribution Measurements

Arnaud Delcorte, and Claude Poleunis

J. Phys. Chem. C, **Just Accepted Manuscript** • DOI: 10.1021/acs.jpcc.9b05363 • Publication Date (Web): 15 Jul 2019

Downloaded from pubs.acs.org on July 30, 2019

Just Accepted

"Just Accepted" manuscripts have been peer-reviewed and accepted for publication. They are posted online prior to technical editing, formatting for publication and author proofing. The American Chemical Society provides "Just Accepted" as a service to the research community to expedite the dissemination of scientific material as soon as possible after acceptance. "Just Accepted" manuscripts appear in full in PDF format accompanied by an HTML abstract. "Just Accepted" manuscripts have been fully peer reviewed, but should not be considered the official version of record. They are citable by the Digital Object Identifier (DOI®). "Just Accepted" is an optional service offered to authors. Therefore, the "Just Accepted" Web site may not include all articles that will be published in the journal. After a manuscript is technically edited and formatted, it will be removed from the "Just Accepted" Web site and published as an ASAP article. Note that technical editing may introduce minor changes to the manuscript text and/or graphics which could affect content, and all legal disclaimers and ethical guidelines that apply to the journal pertain. ACS cannot be held responsible for errors or consequences arising from the use of information contained in these "Just Accepted" manuscripts.

is published by the American Chemical Society. 1155 Sixteenth Street N.W., Washington, DC 20036

Published by American Chemical Society. Copyright © American Chemical Society. However, no copyright claim is made to original U.S. Government works, or works produced by employees of any Commonwealth realm Crown government in the course of their duties.

Mechanistic Insight into Gas Cluster-Induced Sputtering of Kilodalton Molecules using Kinetic Energy Distribution Measurements

Arnaud Delcorte and Claude Poleunis*

Université catholique de Louvain, Institute of Condensed Matter and Nanoscience, 1 Place Louis Pasteur, 1348 Louvain-la-Neuve, Belgium. *Email: arnaud.delcorte@uclouvain.be

ABSTRACT: Recent progress in organic secondary ion mass spectrometry (SIMS) relied essentially on the development of new cluster beams, especially large atomic and molecular clusters formed via the adiabatic expansion of a gas in the vacuum (Ar_n^+, $[CH_4]_n^+$, $[CO_2]_n^+$, $[H_2O]_n^+$). Though computer simulations and a few experimental investigations have shed light on certain fundamental aspects of large cluster-induced molecular desorption, the analytical application of these new beams usually preceded the detailed understanding of their interaction with surfaces. Here, in order to gain insight into the molecular emission process, the axial kinetic energy distributions (KED) of secondary ions emitted from organic films bombarded with $Ar_{330\text{-}5000}^+$ and Bi_5^+ clusters were measured using a reflectron time-of-flight secondary ion mass spectrometer. Irganox 1010 was chosen as a model kilodalton molecule because a large body of SIMS data involving this molecule already exists in the literature. Our results show that the axial KED of Irganox molecular and fragment ions varies as a function of the scaled kinetic energy *E/n* of the Ar cluster projectile, and so does the fraction of ions produced above the surface via unimolecular dissociation, which exhibit an energy deficit with respect to the full acceleration provided at the entrance of the spectrometer. Below a few tens of eV/atom, the KEDs of ions such as $(M-H)^-$ (*m/z* 1175) become gradually narrower and their formation via metastable decay in the gas phase above the surface intensifies. Interestingly, the molecular ion $M^{\cdot+}$ (*m/z* 1176) is essentially produced in the gas phase with both Ar_n^+ and Bi_5^+ cluster beams. Specifics of the observed KEDs of negative and positive molecular ions are discussed in comparison with results of other experiments recently reported in the literature and of molecular dynamics (MD) computer simulations using a coarse-grained representation of kilodalton organic molecules. The measurement of the axial kinetic energy of molecular and fragment ions sputtered from Irganox 1010 under argon and bismuth cluster bombardment, complemented with MD simulations, offers a clearer microscopic view of the emission process.

1. Introduction

In comparison with electrospray ionization (ESI) and matrix-assisted laser desorption ionization (MALDI),[1,2] secondary ion mass spectrometry (SIMS) was traditionally considered as a rather destructive form of mass spectrometry for organic molecules, unable to deliver useful yields of large molecular ions, except in the cases of MeV energy primary ions (plasma desorption mass spectrometry – PDMS) or liquid samples (fast atom bombardment – FAB and liquid SIMS).[3,4] The high degree of fragmentation encountered in SIMS spectra of large (bio)molecules was due to several factors. First, the analytes are probed in the solid state, with reduced mobility and possible molecular entanglement. Second, ion beams with keV energies naturally break numerous chemical bonds and generate energetic recoil atoms when penetrating the surface, causing extensive damage in the sample. Third, the sputtered volume per impact is orders of magnitude smaller than for MALDI. Finally, unlike MALDI, SIMS does not routinely use a matrix to help molecular ionization. However, the smaller analyzed volume and absence of matrix turn out to be decisive advantages for high resolution imaging in two and three dimensions, and the reduced sample preparation/pretreatment makes the characterization of any kind of vacuum-compatible sample straightforward.

In the last decade, the introduction of large noble gas clusters as new ions for SIMS analysis[5,6,7] and molecular depth-profiling[8,9] have eased the second and most limiting condition for preserving molecular information upon sputtering. Experimental results have demonstrated that decreasing the energy per atom (E/n) of the impinging cluster resulted in less fragmented mass spectra,[5,6,10] which was explained by molecular dynamics (MD) computer simulations.[11,12] Kilodalton molecules transferred from a target onto a collector by 10 keV Ar_{2000}^{+} ions showed only minor variations in the recorded mass spectra, with an intense molecular ion in both cases.[13] A transition in the fragmentation behavior was found in the region 10-20 eV/atoms, with a rapidly increasing fragmentation below that region and a stabilization above.[10] Recently, the internal energy distribution of ions sputtered by large Ar clusters could be established using “thermometer” benzylpyridinium ions,[14] according to the survival yield method.[15] For these small molecular ions (~200 Da), a transition was also observed in the mean internal energy (IE) curve as a function of E/n, also located around 10 eV/atoms, with a fast increase of IE before 10 eV and a plateau beyond 10 eV. The IE distributions obtained with the lowest E/n (2-3 eV/atom) are comparable to those measured in ESI and DESI,[15] which are reputed to be much less destructive towards organic molecules. This remarkable study sheds light on the energetics of the process of large Ar cluster induced sputtering (or desorption) and substantiate their success for the 2D and 3D characterization of fragile (bio)molecules such as those found in cells and tissue sections,[7,16,17] in organic electronics multilayers[9] or in complex coatings developed for the industry.[18,19] However, the survival yield method relies on small benzylpyridinium molecules and, to our knowledge, the energetics of emission of large molecules (> kDa) has not been directly studied yet.

In this article, we contribute to a better understanding of kilodalton molecule emission and fragmentation by reporting the axial kinetic energy distributions (KED) of ions sputtered from a model molecule, Irganox 1010™ (1176 Da), under Ar and Bi cluster ion bombardment. The integrals of the energy distributions were obtained by varying the voltage of the reflectron analyzer and transformed into KEDs by a straightforward mathematical procedure. Our results show a dependence of the axial KED of Irganox fragments and molecular ions on the *E/n* of the cluster projectiles and also important variations of the fractions of ions resulting from metastable decay reactions in the vacuum, according to the bombardment conditions and the considered secondary ion. The results are discussed in regards with the recent literature and with new insights provided by MD simulations.

2. Methods

2.1. Samples

Irganox 1010 [octadecyl-3-(3,5-di-*tert*-butyl-4-hydroxyphenyl) propionate] was purchased from Ciba Specialty Chemicals Inc., Basel. The powder sample was dissolved to a concentration of 1 mg/mL in toluene (VWR, Analytical grade, 100%) and spin-cast (initial acceleration: 20 000 rpm s^{-1}; maximum speed: 5000 rpm; total time: 60 s) on clean silicon wafers (~1 cm^2). The Si wafers (Neyco) were rinsed in isopropanol (VWR, HPLC grade, 100%), hexane (VWR, Analytical grade, 99.1%) and toluene (ibidem) prior to spin coating.

2.2. ToF-SIMS

The time-of-flight (ToF) SIMS experiments were performed using an ION-TOF TOF.SIMS 5 (Münster, Germany) instrument equipped with both Bi(Mn) Nanoprobe-LMIG (liquid metal ion gun) and Ar-GCIB (gas cluster ion beam) primary ion sources providing beams oriented at 45° to the surface normal. The secondary ions were extracted by a reflectron-type ToF analyzer in the direction perpendicular to the sample surface. SIMS spectra were acquired in the negative ion polarity for all the bombardment conditions and in the positive ion polarity for only some of them. 30-keV Bi^+ (0.9 pA and Bi_5^+ ions (0.07 pA) were used to collect reference mass spectra of Irganox 1010 that could be compared to the literature. For these bombardment conditions, the mass resolving power at *m/z* 29 ($C_2H_5^+$) was around 5,000 which is sufficient to resolve the hydrocarbon from the O-containing ions in the low mass region. The Ar cluster source is equipped with a 90° pulsing system for mass separation by momentum deflection.[20] The mass resolution of the system is $m/\Delta m$=60 – 120. The pulsing system also allows the variation of the applied cluster size out of the large cluster size distribution, ranging from 250 to 10000 atoms.[6] The beam conditions used in this study are listed in Table 1. All the mass spectra were collected from a 500 x 500 μm² area, with no charge compensation to prevent any undesired influence on the measurements. The sample coatings were sufficiently thin to avoid any detectable charging effect on the results.

For the kinetic energy distribution measurements, a sequence of maximum 12 mass spectra was recorded on the same sample area, corresponding to maximum cumulated ion doses of 1.6×10^{12} ions/cm² for 30-keV Bi^+ and 2.5×10^{11} ions/cm² for 30-keV Bi_5^+, much less for the Ar cluster measurements where the AC current was not always measurable. To obtain a sufficient number of data points and test reproducibility, successive series of acquisitions were performed on two or three different areas of each analyzed sample. In order to record the integral of the axial kinetic energy distribution, the reflectron was used as low-pass filter, allowing the ions with an axial energy $E_k < E_r$ (with $E_r = e^*V_r$ and V_r being the reflector voltage) to be reflected and collected on the detector, as was proposed by Brison.[21] V_r was varied over a range of ~50 V around the reference value and SIMS spectra were recorded for each voltage. The curve reporting the measured intensity of an ion as a function of voltage should then mirror the integral of the axial KED of that particular ion,[22] a 1 V change of V_r corresponding to a 1 eV change of the ion energy. The obtained data were not corrected for the 0.75 degree tilt of the analyzer. In the TOF.SIMS 5, the analyzer lens placed right after the extractor may also modify the axial KED by partially converting radial into axial energy (up to an estimated 0.5 eV given the considered angular distributions for 45° Ar_n^+ bombardment). This effect is not corrected either and must be kept in mind while interpreting the results. The zero of the energy distributions was calibrated using the signals of atomic ions, for which metastable decay is almost absent (Si^+ and H^+ in the positive polarity and O^- and H^- in the negative polarity). Once energy calibration was achieved, the fraction of daughter ions produced above the surface as a result of the metastable decay of larger parent ions was directly obtained from the selected ion intensity measured for V_r below zero.

Table 1. List of the projectile characteristics and the corresponding features of the KEDs of the $(M-H)^-$ ions sputtered from Irganox 1010.

Projectile			***$(M-H)^-$ energy distribution***	
Nature	**E (keV)**	**E/n (eV)**	**FWHM (eV)**	**Metastable (%)**
Mn^+	30	30000	1.74	14
Bi^+	30	30000	1.67	10
Bi_5^+	30	6000	1.73	30
Ar_{330}^+	20	60.6	1.74	35
Ar_{700}^+	20	28.6	1.80	37

Ar_{700}^+	10	14.3	1.75	32
Ar_{1500}^+	10	6.7	1.64	39
Ar_{3000}^+	20	6.7	1.60	41
Ar_{5000}^+	20	4	1.40	41
Ar_{3000}^+	10	3.3	1.39	45
Ar_{5000}^+	10	2	1.18	55

2.3. Data processing

The result of the integral KED measurement and the energy distribution obtained after data processing are shown in Fig.1 for Si^+ ions sputtered from a clean silicon wafer. The measured data were fitted with the integral of two functions commonly used for the description of kinetic energy distributions in the SIMS community. For atomic ion distributions such as Si^+, the Sigmund-Thompson function was used, $n(E_k) \sim E_k/(E_k+U)^3$ {Eq. 1}; where the parameter U is the binding energy at the surface.[23,24] For polyatomic ion distributions, including the fragments and the molecular ions of Irganox 1010, a Maxwell-Boltzmann distributions was preferred.[25,26] The form of the Maxwell-Boltzmann distribution for the energy is $n(E_k) = 2(E_k/\pi)^{0.5} (1/kT)^{1.5} \exp(-E_k/kT)$ {Eq. 2} (see for example Ref. 27 for derivation). Both functions can be easily integrated analytically and their integrals were used to perform a least square regression on the measured data (shown in Fig.1, dashed line, for the integral of the Sigmund-Thompson function). A constant value corresponding to the 0 V signal (i.e. the integral of the signal of ions produced above the surface) was added to the integral for the fit. U in Eq. 1 and T in Eq. 2 were used as fitting parameters. These two functions were found to fit adequately all the measured integral distributions beyond 0 V. Fig.1 also shows the actual Sigmund-Thompson function (solid line) corresponding to the derivative of the regression function.

2.4. MD simulations

The molecular dynamics simulation program used in this study was the SPUT code developed by the group of B.J. Garrison at Penn State University for sputtering applications.[28] In the classical MD method, Hamilton's equations of motion are numerically integrated over a given time interval, providing us with the position and velocity of each particle at each timestep. Forces among the atoms or particles in the system are derived from empirical interaction potentials. The organic target used in this study and the methodology of coarse-graining have been described in detail in previous articles.[29,30] In order to gather sufficient statistics on molecular emission, icosane molecules (formula: CH_3-$(CH_2)_{18}$-CH_3 – mass 282 Da) were chosen to form a solid sample. The target was made of united atoms of CH_2 (14 amu) and CH_3 (15 amu) in order to reduce computational expense. The interaction potentials were Lennard-Jones potential functions for intermolecular (nonbonding) interactions, and Morse potential functions for the intramolecular (covalent) interactions in the chains.[31] Ar clusters were modeled using Lennard-Jones potentials splined to the KrC repulsive potential at short interdistance.[11] A purely repulsive Molière potential was used to describe the Ar-icosane interactions. In all the simulations, the projectile incidence angle was 45°. The trajectories were run for a minimum of 25 ps, up to saturation of the sputtered flux. Full sets of simulations using Ar_n clusters with energies between 2.5 and 10 keV were conducted using a damping zone at the bottom and on the four lateral sides of the sample (Langevin algorithm with a friction coefficient), in order to absorb the pressure waves and mimic a semi-infinite, bulk sample. Because of the simplicity of the chosen approach and potentials, the sample should be considered as a generic model of an amorphous organic solid made of long-chain molecules rather than strictly alkanes. In addition, the number of covalent bonds is reduced by a factor of

~3 with this method, which probably affects the distribution of energy between translational and internal modes upon sputtering.

3. Results and Discussion

3.1. Atomic and small fragment ions

The main goal of this article is to investigate the sputtering process of organic samples by large Ar clusters via the interpretation of the energy distributions of their secondary ions. However, prior to that, the methodology of the KED measurement with the reflectron analyzer of the TOF.SIMS 5 was established using 30 keV Bi_5^+ ions produced by the liquid metal ion source, which generally provides a higher and stable current and a much better mass resolution of the spectra than large Ar clusters. In terms of samples, clean silicon wafers were selected as reference because they are very flat and conducting, therefore avoiding any possible difficulties related to surface topography or charging. The measured integral KED of Si^+, its fit by the integral of a Sigmund-Thompson distribution and the corresponding derivative are shown in Fig. 1. The surface binding energy value U provided by the fit is 4.8 eV. It is about half the value obtained in previous measurements conducted on a Physical Electronics instrument equipped with a triple electrostatic (TRIFT™) analyzer where the total translational energy was recorded (with also some influence of the angular distribution). In contrast, our current experiment should provide the axial energy of the ions and therefore, the value of U deduced from the fit should underestimate the actual value obtained from a distribution of the total translational energy. In addition, one cannot exclude an influence of the different bombardment conditions. Despite the differences, the fit of the integral KED with a Sigmund-Thompson function is adequate and the KED of Si^+ displays the usual characteristics of atomic ion energy distributions (sharp rise to the maximum, high energy tail).

The axial KEDs of positive and negative ions sputtered from an ultrathin film of Irganox 1010 spin-cast on silicon were then measured. These measurements were also performed without any charge compensation by electron floodgun. The good stability and reproducibility of the measurements indicate that charging is not an issue for those samples where the Si substrate remains visible in the mass spectra (presence of Si^+, $SiOH^+$, SiO_3H^-). Figure 2 presents the KED of small hydrocarbon fragments of the form $C_2H_y^+$ measured under 30 keV Bi_5^+ bombardment (fit with a Maxwell-Boltzmann distribution). The energy distributions of these ions are known to be governed by their degree of unsaturation, or more precisely, by the deficit in hydrogen with respect to the initial structure of the molecule.[32,33] In the case of Irganox 1010, a large fraction of the $C_2H_y^+$ ions must arise from the fragmentation of the eight butyl functional groups. As was previously observed for a series of hydrocarbon and more complex organic samples upon atomic ion bombardment (12 keV Ga^+ and Cs^+), the widths of the $C_2H_y^+$ ion distributions gradually increase with decreasing H content, from 0.5 eV for $C_2H_5^+$ to 5 eV for C_2H^+.[32] Though these values cannot be systematically compared given the different bombardment and measurement conditions, the trend is similar. The interpretation was that more fragmented ions (larger H losses with respect to the molecular precursor) receive more energy (kinetic+internal) to be formed and, while fragmentation by H-loss changes the internal energy of the decaying ion, it should little affect the kinetic energy because of the comparatively small mass of hydrogen. Small H-deficient ions are then produced by energetic collisions, probably in the hot part of the energized volume, and this is mirrored by the width of their KED. Strongly H-deficient and/or fragmented hydrocarbon ions such as C_2H^+, $C_2H_2^+$, C_3H^+, $C_3H_2^+$ are also much less abundant, or even absent from the mass spectra obtained upon large Ar cluster bombardment. The fragmentation of Irganox 1010 and other molecules upon Ar_n^+

cluster bombardment, and its dependence on cluster size and energy, was analyzed in detail by Seah et al.[34] Table 2 compares the $C_xH_y^+$ ion intensities relative to the most intense of the series (same *x*, different *y*), for 30 keV Bi_5^+ and 10 keV Ar_{3000}^+ bombardment. While the difference of secondary ion abundance between the two beams is small for ions which have a narrow KED, it reaches one order of magnitude or more for those which have a broad KED, such as C_2H^+ and $C_2H_2^+$. The fact that these ions are seldom observed upon mild bombardment conditions (Ar_{3000}^+) is consistent with the hypothesis that they are more efficiently formed in a hotter cascade core,[35] such as the one induced by Bi_5^+, resulting in comparatively higher average kinetic energies.

Table 2. Relative abundance of $C_xH_y^+$ ion sputtered by 30 keV Bi_5^+ and 10 keV Ar_{3000}^+ ions.

Primary ions – Energy	Secondary ions (in % of $C_xH_5^+$ intensity)				
	C_2^+	C_2H^+	$C_2H_2^+$	$C_2H_3^+$	$C_2H_5^+$
Bi_5^+ – 6 keV/at.	0.1	0.09	1.4	29	100
Ar_{3000}^+ – 3.3 eV/at.	-	-	0.11	21	100
	C_3^+	C_3H^+	$C_3H_2^+$	$C_3H_3^+$	$C_3H_5^+$
Bi_5^+ – 6 keV/at.	0.01	0.31	1.5	31	100
Ar_{3000}^+ – 3.3 eV/at.	-	0.02	0.21	28	100

From the methodological viewpoint, it is also interesting to note that the integral measurement using the reflectron (this study) provides us with a better energy resolution than the measurement conducted with the TRIFT™ analyzer, by inserting an energy slit with a limited resolution (100 μm corresponding to 1.5~2 eV) at the crossover following the first electrostatic analyzer. This is indicated by the KED of $C_2H_{3-5}^+$ which are significantly thinner than 2 eV, while all the distribution widths were converging towards ~2 eV for the most saturated $C_xH_y^+$ ions in previous measurements.[32,33]

3.2. Large fragments and molecular ions

When the energy per atom of the Ar cluster projectiles decreases, the mass spectra of organic samples become less and less fragmented.[5,10,12] Here, we focus on the effect of the cluster energies E and nuclearities n on the kinetic energy of large organic ions. First, $(M\text{-}H)^-$ ions (*m/z* 1175) are observed in all the investigated bombardment conditions (Table 1). The measured integral KEDs of $(M\text{-}H)^-$ are shown in Fig. 3a for a selection of projectiles and impact energies. The integral curves gradually shift to higher voltages (energies) as E/n increases and they tend to converge at high E/n. For instance, the integral KEDs of 20 keV Ar_{700}^+ and 30 keV Bi_5^+ are quite similar except for the "negative" voltage part which corresponds to ion formation in the gas phase, at some distance above the surface. Not surprisingly, this evolution is mirrored by the Maxwell-Boltzmann distributions derived from these curves, Fig. 3b. The distribution widths increase with E/n, from 1.2 to 1.8 eV (Table 1). In order to have a complete view of the effect, the full widths at half maximum (FWHM) of the axial KED of $(M\text{-}H)^-$ ions are plotted in Fig. 4a for all the bombardment conditions tested in this study. The widths of the distributions increase steeply from 2 to 10 eV per atom, then the slope changes up to a maximum around 30 eV per atom. Beyond 30 eV, the widths seem to decrease slightly, but the variation remains within the estimated ±0.05 eV error (experimental uncertainty + fitting). As for previous investigations of ion yields and internal energies,[14,36,37] the representation of the axial KED widths as a function of the scaled projectile energy (per atom or per nucleon), or the square of their velocity v^2, is justified by the fact the projectiles with different nuclearities n but similar E/n produce very similar results. It is, for instance, the case for 20 keV Ar_{3000}^+ and 10 keV Ar_{1500}^+, or for 20 keV Ar_{5000}^+ and 10 keV Ar_{3000}^+. Within the measurement error, our data describe a single curve as a function of E/n.

Irganox dimers are also observed with sufficient intensity in the SIMS spectra obtained under Bi_5^+ bombardment so that their KED can be measured, but it is generally not the case for large Ar_n^+ ion bombardment. Though the beam current is often lower with Ar clusters, there might be another reason, because when decreasing E/n, the ratio of the dimer to the monomer intensity also decreases, which is at odds with observations made on smaller molecules (amino acids).[10] Figure 5 shows the integral KEDs and their respective Maxwell-Boltzmann distributions for the deprotonated monomer and dimer of Irganox under 30 keV Bi_5^+ impact. In spite of the experimental uncertainty, the axial KED of the dimer is significantly broader than the one of the deprotonated monomer. Broader energy distributions were also observed for dimers than for monomers in the case of triacontane samples bombarded by 12 keV Ga^+ ions (15 kV of acceleration minus 3 kV corresponding to the sample bias in the positive ion polarity).[38]

3.3. Ion formation in the gas phase

The “negative” voltage part (with respect to the reference corresponding to the 2 kV acceleration voltage) of the axial energy distributions provides us with information about ions which do not have the full acceleration energy. Since ionization far from the surface should be negligible, it can be assumed that these ions are produced by metastable decay of larger parent ions in the acceleration section or the field-free drift region of the spectrometer.[22,39,40,41] Polyatomic secondary ions which loose a neutral atom or molecule in those regions also loose a fraction of kinetic energy proportional to the mass of the neutral loss, thereby appearing as signal corresponding to a “negative” voltage or energy in our measurements. As an example, a monomer ion of Irganox with a 4 eV energy deficit, resulting from the decay of a charged dimer, would correspond to a dissociation reaction occurring ~6 µm above the surface in our instrument (2 kV over ~1.5 mm). In this work, the fraction of ions produced by unimolecular dissociation in the gas phase was simply estimated by the signal of the integral KED measured at 0 V divided by the maximum signal. In the normalized curves, the fraction of ions formed above the surface is directly given by the 0 V signal.

As was observed in previous works, atomic ions generally display very little formation in the vacuum via metastable decay reactions. It is the case for Si^+ (Fig. 1), but also O^-, H^- and H^+ emitted from Irganox 1010. For small $C_2H_y^+$ fragment ions such as those shown in Fig.2, the fraction of ions produced in the gas phase increases with the H-content y, up to 47% for $C_2H_5^+$. A similar effect was observed for 12 keV Ga^+ bombardment of polyisobutylene, a saturated hydrocarbon polymer.[41]

The integral KEDs of $(M-H)^-$ ions, Fig. 3a, indicate that the bombardment conditions also influence the proportion of ions arising from metastable decay reactions. This fraction increases with decreasing E/n, meaning that for a given projectile energy, it increases with the projectile size. Nevertheless, Fig. 4b and Table 1 show that the fraction produced in the gas phase varies slowly beyond 10 eV/atoms. The variation is more pronounced between 1 and 10 eV/atoms. The inset of Fig. 3a shows the negative part of the integral KEDs renormalized to the value of the signal at 0 V. After renormalization, the curves appear to be similar, within the experimental uncertainty, indicating that the dynamics of the unimolecular dissociation does not depend strongly on the bombardment conditions. Only the relative fraction of $(M-H)^-$ ions produced in the vacuum does. This suggests that the amount of precursors changes more markedly than their internal energy distributions, since a significant change of internal energy should modify the decay constant and lead to different slopes in the negative part of the KEDs. Therefore, one can say that the fraction of metastable precursor ions of $(M-H)^-$, possibly charged dimers or multimers of Irganox, relative to the fraction produced at the surface, increases significantly with E/n in the energy range of 0 to 10 eV/atom.

Figure 5 also demonstrates that 50 % of dimer ions are formed in the gas phase against 30% of the monomers $(M-H)^-$, for 30 keV Bi_5^+ bombardment. The inset, with the renormalized curves as in Fig. 3a, shows that the signal decays faster for the monomer $(M-H)^-$ than the dimer ion as a function of voltage, i.e. as a function of distance from the surface. Since the average velocities of sputtered polyatomic ions usually decrease with increasing size (as is verified here for the dimer with respect to the monomer, though the average *kinetic energies* slightly increase, Fig. 5), dissociation reactions occurring farther from the surface for dimers also mean larger times or smaller decay rates, i.e. larger internal energy densities.[1] This could suggest that the parents of dimer ions originate in a region more remote from the impact point than those of monomers (lower internal energy), or that they can accommodate a higher energy density (higher energy barrier for dissociation). The second possibility seems unrealistic, especially if multimers are non-covalent complexes. Because the KED measurements do not provide any precise information on the nature of the parent ions giving rise to the observed daughter ions, our interpretations can only remain conjectural.[41]

The integral KED of positive ions has also been analyzed, Fig. 6. The case of the positive molecular ion of Irganox 1010, $M^{\cdot+}$, is remarkable, because ~90 % of the $M^{\cdot+}$ are formed in the gas phase, and not at the surface, under 30 keV Bi_5^+ bombardment, and >90% for 10 keV Ar_{3000}^+ bombardment. Given the nature of this ion, one must assume that it arises from the decomposition of multimers, which are not observed in the positive SIMS spectra. In the case of $(M-H)^-$, there was a clear indication of two major formation channels, direct emission of the ion from the surface, corresponding to a rather energetic process, and formation in the gas phase, resulting from the softer emission of larger entities. For $M^{\cdot +}$, the second channel corresponding to the emission of clusters from a region of lower energy density, is by far the main channel, irrespective of the projectile, while the higher energy channel of emission from the surface appears almost negligible. The reason why dimers or higher order multimers are seldom observed remains difficult to explain, but their small binding energy might explain their full collapse before reaching the detector. An alternative possibility could be that globally neutral dimers give rise to a positive and a negative monomer in the gas phase. In contrast, the KED of the large fragment at *m/z* 219, $[CH_2-(C_6H_2)-(C_4H_9)_2-OH]^+$ indicates more decomposition in the gas phase for Bi_5^+ impacts than Ar_{3000}^+ impacts. For CH_3^+, the results are similar with the two ion beams (~40%), showing the diversity of scenarios. H^+ is emitted only from the surface under Bi_5^+ bombardment and almost no protons are emitted by 10 keV Ar_{3000}^+ clusters. Finally, it should be noted that the slopes of the integral KEDs obtained with Ar_{3000}^+ are steeper than with Bi_5^+, which translates in thinner energy distributions. This observation, made here for positive fragment ions, is consistent with what we observed for negative molecular (Fig. 3) and fragment ions (not shown).

3.4. Molecular dynamics simulations

In previous articles, we have demonstrated that a coarse-grained model of hydrocarbon oligomers could be used to model the main trends of the sputtering yields of organic materials under cluster bombardment, especially argon Ar_n^+ and fullerene C_{60}^+ clusters.[11,12,30] In particular the yields of Irganox 1010, taken from the compilation of Seah,[37] were predicted almost quantitatively with polyethylene oligomers of a similar mass, as well as the angular effect, from 45° to 0° (normal) projectile incidence.[11] This is mainly due to the fact that the density and the cohesive energy of the solid (especially the intermolecular potential) are reasonably described. However, because of the simplicity of the model, it is not expected that the kinetic energy of the sputtered molecules should be quantitatively described. Several arguments can be invoked including the (i) classical nature of the model, (ii) the selected model molecules, (iii) the temperature (0 K), (iv) the absence of ionization, (v) the reduced number of degrees of freedom able to store internal energy (coarse-graining[30]), or (vi) the very short timescale (<50 ps) preventing most metastable decay reactions to happen. While (i-iii) didn’t seem to prevent a rather good prediction of the sputter yields, (iv-vi) should naturally influence the internal and kinetic energy distributions of the sputtered ions. Nevertheless, the results shown hereafter give us good reasons to think that, if quantitative values of the sputtered molecule energies are out of reach of our model, at least the main trends observed in the experiments can be predicted.

As was explained in the method section, the model sample is an amorphous solid made of icosane molecules, which was bombarded by Ar clusters with nuclearities n ranging from 18 to 5000 and energies E between 2.5 and 10 keV, allowing us to cover a range of E/n from 0.5 to 556 eV. Icosane, significantly smaller than Irganox 1010, was selected for this study because much more molecules are emitted per impact than for heavier molecules, so that only one impact per bombardment condition was sufficient to collect reasonable statistics, making these simulations tractable. Figure 7a shows the average axial kinetic energy of icosane molecules sputtered by Ar cluster impacts, as a function of the scaled energy E/n. Even though the data points are scattered in the high energy range, the evolution of the average axial energy of the molecules for $0.5 < E/n < 10$ is striking and, overall, the trend observed in the experimental results is reproduced (Fig. 4a). The average axial energy increases steeply up to a certain value of E/n (~10 eV in the simulations, somewhat more in the experiments), then it seems to reach a plateau. Unlike the experiments, the simulations also give us access to the total kinetic energy of the molecules, Fig. 7b. Again, the data points are scattered, but an increase of the kinetic energy at low *E/n* can be observed, followed by a decrease after the maximum. The stabilization of the axial kinetic energy beyond the maximum therefore corresponds to a decrease of the total kinetic energy and, in turn, to emission angles which should become closer to the normal. Using the same data, the average emission angles were calculated and plotted in Fig. 7c. Interestingly, the resulting angles merge very nicely in a curve of decreasing emission angle with increasing *E/n* with, perhaps, a slight change of slope around 20 eV/atom.

Snapshots of the molecular dynamics help understand the microscopic phenomena. Figure 8 shows side views of the impact and sputtering events at different times and for two very different bombardment conditions, 5 keV Ar_{18} – 278 eV/atom, in red, and 5 keV Ar_{5000} – 1 eV/atom, in blue (grey circles in Fig. 7). The time evolution of the sputtering event shows that Ar_{5000} ejects only intact molecules and in the forward direction, which explains very simply the emission angle reported in Fig. 7c. Such a forward-directed ejection was observed for large clusters in previous theoretical[42,43,44] and experimental[13] studies. In contrast, isoenergetic Ar_{18} ejects a large number of single atoms, fragments and intact molecules and the plume displays an almost radial symmetry in spite of the off normal incidence angle. This is typical of smaller energetic clusters such as Bi_n, C_{60} or Ar_n.[45] Indeed, for rather small kiloelectronvolt clusters such as C_{60}, the development of the collision cascades in organic solids is only slightly affected when going from normal to 45° incidence.[46] For information, Table 3 provides the distribution of the ejected plume between intact icosane molecules and fragments under 5 keV Ar_n bombardment, the two extreme cases being those described in Fig. 8.

A subset of trajectories involving different cluster sizes and energies were reanalyzed more quantitatively in order to gain a better understanding of the transition observed in the experimental results and in the MD simulations. To do so, the reaction of the icosane solid upon impact was investigated in detail. In particular, Figure 8e shows the velocity of the pressure waves induced in the solid for different bombardment conditions, as a function of the scaled kinetic energy of the projectile, *E/n*. The measure of the pressure wave velocities was obtained be reporting the forward (x) and downward (z) positions of the wave fronts as a function of time and then fitting the data with linear functions, whose slopes provided the velocities. Figure 8e shows that the pressure wave velocities first increase with *E/n*, from ~2 to ~5 km/s around 10 eV/atom, then decrease after a broad maximum. Therefore, the pressure wave velocities also show a clear transition region around 10-40 eV/atom for icosane samples, which is reflected in the sputtered molecule energies and emission angles, and indicates two different physical situations of cluster impact. As a reference, the measured speed of sound in n-hexadecane is ~1.3 km/s and for polyethylene, ~2 km/s, so that the pressure wave velocities measured for slow projectile impacts are close to the speed of sound in the solid. With increasing projectile velocity, they become clearly supersonic. Beyond the maximum, one enters the region of fast cluster impacts, where the projectile and wave velocities decouple, in the sense that the wave velocity decreases while the projectile speed upon impact continues to increase. It is also the region where fragmentation starts to increase significantly, finally reaching ~30% of the total sputtered mass for 5 keV Ar_{18} (Table 3). The relationship between the pressure wave and projectile velocities is best shown by their ratio (component of the wave front velocity along the forward direction x divided by the cluster velocity along the same direction, in red in Fig. 8e). At low impact velocity, the ratio is close to 2, meaning that the pressure wave speed is twice faster than the impact velocity in the forward direction (in binary elastic collisions, a situation encountered when a massive body encounters a very light one). Then the ratio decreases and falls below 1 (identical forward velocities) around 10 eV/atom, where the transition region starts. It continues to decrease quickly afterwards (0.17 for 5 keV Ar_{18}). In summary, the detailed analysis of the dynamics confirms the change occurring around 10 eV/atom, a transition between slow clusters with velocities commensurate with the reaction times of the material and fast clusters shattering upon impact, which induce supersonic pressure waves in the solid, but with a trend of decreasing wave speed with increasing *E/n*.

Table 3. Distribution of the sputtered mass as a function of the nature of the ejecta in the MD simulations of icosane bombardment, for a selection of projectiles with 5 keV of kinetic energy.

Projectile (*E/n*)	**Mass of intact molecules: *A* (kDa)**	**Mass of fragments: *B* (kDa)**	**% of intact molecules: *A/(A+B) x 100***
Ar_{5000} (*1 eV*)	13.8	0.02	0.1
Ar_{3000} (*1.67 eV*)	24.5	0.04	0.2
Ar_{1000} (*5 eV*)	37.8	0.06	0.2
Ar_{500} (*10 eV*)	34.4	0.9	2.4
Ar_{250} (*20 eV*)	35.0	4.0	10.2
Ar_{60} (*83.33 eV*)	30.7	9.6	23.8
Ar_{18} (*277.78 eV*)	29.6	13.4	31.1

Finally, the experimental (this article and [13,14]) and simulation results provide us with a composite yet consistent picture of molecular emission induced by cluster projectiles, which is a function of their scaled energy per atom (*E/n*). Two or three regions of *E/n* can be identified. Before a transition region located around 10-30 eV/atom, both the axial kinetic energy and the internal energy of the sputtered molecules increase steeply with *E/n*. Below 10 eV/atom, molecular fragmentation can therefore be tuned by the *E/n* of the projectile, which explains the observations of softer sputtering or desorption generally reported for large Ar clusters.[5,10] The transition region corresponds to a maximum of the total kinetic energy of the sputtered molecules (and their velocities). Beyond the transition, the axial kinetic energy and the internal energy vary little over a very wide range of *E/n* (3 decades according to Fig. 4a and [14]). In agreement with the very similar internal energy distributions measured over that range of *E/n*, the fraction of $(M-H)^-$ ions produced by metastable decay in the vacuum is almost constant (Fig. 4b). However, in that region, the simulations indicate a trend of decreasing total kinetic energy with *E/n* that is accompanied by a slow decrease of the emission angle (Fig. 7b-c). For 45° bombardment of Irganox 1010 with 10 keV Ar_{2000}^+, Lorentz et al. measured an angular distribution of the sputtered material peaking at 65°, while our simulations suggest an average angle of ~55° for the same *E/n*. In addition to the acknowledged differences between the model and the experiments, they measured the distributions via the redeposited material, which probably includes both intact and fragmented molecules, making a direct comparison difficult. However, the increase of the average emission angle with increasing cluster size *n* was pointed in the literature, due to the blocking of normal emission by very large projectiles.[44]

4. Conclusion

The axial kinetic energy distribution measurements conducted in this study help us build a more complete view of the molecular and fragment ion emission from organic samples (here, Irganox 1010) bombarded by large noble gas clusters. They show a pronounced dependence of the deprotonated molecular ion axial energy on the energy per atom (*E/n*) of the projectile below 10 eV, as well as a concomitant dependence of their formation via unimolecular dissociation in the gas phase (up to 55% of the $(M-H)^-$ abundance at 2 eV/atom). The reduction of the axial kinetic energy with decreasing *E/n* is also observed for fragment ions mirroring the molecular structure of Irganox (CH_3^+, *m/z* 219^+, 231^-, etc.) The observed evolutions, supported by MD simulations and internal energy distribution measurements performed with small molecules,[14] confirm that there exists a transition around 10-30 eV/atom, beyond which the axial kinetic energy and the internal energy remain essentially constant, over 3 decades of *E/n*, with only a slight decrease of the total kinetic energy and the emission angle with respect to the normal. In parallel, our results demonstrate that ≥90% of the molecular ions $M^{\cdot+}$ are produced in the gas phase irrespective of the bombardment conditions.

Atomic and small fragment ions, such as $C_xH_y^+$ with a hydrogen deficit with respect to the molecular structure, exhibit broad axial energy distributions (5 eV FWHM for C_2H^+) and are depleted or absent at small *E/n*, indicating that the lower energy density at the surface is insufficient for their formation in these conditions.

The energy region below 10 eV/atom would deserve more investigations, and in particular with other types of projectiles, including molecular clusters. Simulation results predict a similar break in the sputtering curve for CH_4 molecular clusters, with decreasing fragmentation below 30 eV/molecule. In that energy range, the CH_4 molecules essentially keep their integrity upon impact, however, experiments with H_2O clusters show that biomolecule protonation can be strongly enhanced around 3 eV/molecule,[47] making that energy region all the more interesting for 2D and 3D molecular imaging by SIMS.

Finally, this fundamental study suggests a few practical remarks. (1) Molecular depth profiling, in order to be as soft as possible, should always be operated in the region below 10 eV/atom, however, this is also the region of non-linear evolution of the sputter yields (Table 3, Refs. 11,34,48), so, depending on the material, a compromise should be found in order to keep damage minimal and sputter yield reasonable. (2) Beyond the sputtering yields, this study indicates that the energetics of ion emission mainly depends on *E/n*, therefore, experiments scaling *E* and *n* proportionally should provide qualitatively comparable mass spectra. (3) At low *E/n*, unimolecular dissociation reactions after emission increase significantly, leading to more ions with an incomplete acceleration and possible peak broadening. Delayed extraction could help improve the situation by giving most metastable ions enough time to decay before being accelerated. (4) Experiments where the sputtered plume geometry matter (SNMS, soft-landing, etc.) should take into account the pronounced variation of emission angle as a function of *E/n*. (5) In molecular transfer experiments, the observed variation of the kinetic energy of the sputtered molecules with *E/n* (Fig. 4) should provide some degree of control of the soft or reactive landing conditions.

Acknowledgements

The authors wish to thank Dr. Derk Rading (ION-TOF GmbH) for useful discussions concerning the KED measurements. This work is supported by the Fédération Wallonie Bruxelles, through the project "iBEAM" funded by its research program "Actions de Recherche Concertées". A.D. is a Research Director at the Fonds National de la Recherche Scientifique (FNRS) of Belgium.

References

---

(1) de Hoffmann, E.; Stroobant, V. Mass spectrometry: principles and applications, J. Wiley & Sons Ltd., Chichester, 2007.

(2) Heeren, R. M. A. Getting the picture: The coming of age of imaging MS. *Int. J. Mass Spectrom.* **2015**, *377*, 672–680.

(3) Standing, K. G.; Ens, W. (Eds.) Methods and mechanisms for producing ions from large molecules, NATO ASI series, Series B: Physics Vol. 269, Plenum Press, New York, 1991.

(4) Sigmund, P. (Ed.), Fundamental processes in sputtering of atoms and molecules, Mat-Fys Medd K Dan Vidensk Selsk 43, Copenhagen, 1993.

(5) Ninomiya, S.; Nakata, Y.; Ichiki, K.; Seki, T.; Aoki, T.; Matsuo, J. Measurements of secondary ions emitted from organic compounds bombarded with large gas cluster ions. *Nucl. Instr. and Meth. Phys. Res. B* **2007**, *256*, 493–496.

(6) Kayser, S.; Rading, D.; Moellers, R.; Kollmer, F.; Niehuis. E. Surface spectrometry using large argon clusters. *Surf. Interface Anal.* **2013**, *41*, 131–133.

(7) Angerer, T. B.; Blenkinsopp, P.; Fletcher, J. S. High energy gas cluster ions for organic and biological analysis by time-of-flight secondary ion mass spectrometry, *Int. J. Mass Spectrom.* **2015**, *377*, 591–598.

(8) Ninomiya, S.; Ichiki, K.; Yamada, H.; Nakata, Y.; Seki, T.; Aoki, T.; Matsuo, J. Precise and fast secondary ion mass spectrometry depth profiling of polymer materials with large Ar cluster ion beams. *Rapid Commun. Mass Spectrom.* **2009**, *23*, 1601–1606.

(9) Mouhib, T. ; Poleunis, C.; Wehbe, N.; Michels, J. J.; Galagan, Y. ; Houssiau, L.; Bertrand, P.; Delcorte, A. Molecular depth profiling of organic photovoltaic heterojunction layers by ToF-SIMS: comparative evaluation of three sputtering beams. *Analyst*, **2013**, *138*, 6801-6810.

(10) Gnaser, H.; Ichiki, K.; Matsuo, J. Strongly reduced fragmentation and soft emission processes in sputtered ion formation from amino acid films under large Ar_n^+ ($n \leq 2200$) cluster ion bombardment. *Rapid Commun. Mass Spectrom.* **2012**, *26*, 1–8.

(11) Delcorte, A.; Debongnie, M. Macromolecular sample sputtering by large Ar and CH_4 clusters: elucidating chain size and projectile effects with molecular dynamics. *J. Phys. Chem. C* **2015**, *119*, 25868-25879.

(12) Delcorte, A.; Cristaudo, V.; Lebec, V.; Czerwinski, B. Sputtering of polymers by keV clusters: Microscopic views of the molecular dynamics. *Int. J. Mass Spectrom.* **2014**, *370*, 29–38.

(13) Lorenz, M.; Shard, A.G.; Counsell, J. D. P.; Hutton, S.; Gilmore, I.S. Angular distribution of molecules sputtered by gas cluster ion beams and implications for secondary neutral mass spectrometry. *J. Phys. Chem. C* **2016**, *120*, 25317-25327.

(14) Fu, T.; Della-Negra, S.; Touboul, D.; Brunelle, A.; Internal energy distribution of secondary ions under argon and bismuth cluster bombardments: soft versus hard desorption–ionization process. *J. Am. Soc. Mass Spectrom.* **2019**, *30*, 321-328.

---

(15) Nefliu, M.; Smith, J. N.; Venter, A.; Cooks, R. G. Internal energy distributions in desorption electrospray ionization (DESI). *J. Am. Soc. Mass Spectrom.* **2008**, *19*, 420-427.

(16) Shon, H. K.; Yoon, S.; Moon, J. H.; Lee, T. G. Improved mass resolution and mass accuracy in TOF-SIMS spectra and images using argon gas cluster ion beams. *Biointerphases* **2016**, *11*, 02A321.

(17) Passarelli, M. K.; Pirkl, A.; Moellers, R.; Grinfeld, D.; Kollmer, F.; Havelund, R.; Newman, C. F.; Marshall, P.S.; Arlinghaus, H.; Alexander, M.R. et al.; The 3D OrbiSIMS —label-free metabolic imaging with subcellular lateral resolution and high mass-resolving power. *Nature Meth.*, **2017** 14, 1175–1183.

(18) Renaud, A.; Bonnaud, L.; Dumas, L.; Zhang, T.; Paint, Y.; Fasano, F.; Kulyk, O.; Pospisilova, E.; Nysten, B.; Delcorte, A. et al. A benzoxazine/substituted borazine composite coating: A new resin for improving the corrosion resistance of the pristine benzoxazine coating applied on aluminum. *Eur. Polymer J.* **2018**, *109*, 460–472.

(19) Cristaudo, V.; Merche, D.; Poleunis, C.; Devaux, J.; Eloy, P. ; Reniers, F.; Delcorte, A. Ex-situ SIMS characterization of plasma-deposited polystyrene near atmospheric pressure. *Appl. Surf. Sci.* **2019**, *481*, 1490–1502.

(20) Niehuis, E.; Heller, T.; Feld, H.; Benninghoven, A. Secondary Ion Mass Spectrometry SIMS V, Springer Series in Chemical Physics 44, A.Benninghoven, (Eds: R. J. Colton, D. S. Simons, H. W. Werner), Springer Verlag, Berlin, 1986, 188.

(21) Brison, J. On the understanding of ionization and cluster formation processes during ToF-SIMS depth profiling by co-sputtering cesium and xenon. PhD thesis, Presses Universitaires de Namur, 2007.

(22) Zubarev, R.A.; Abeywarna, U.; Hakansson, P.; Demirev, P.; Sundqvist, B. U. R. Kinetic energies of secondary ions in MeV and keV particle-induced desorption. *Rapid. Commun. Mass Spectrom.* **1996**, *10*, 1966-1974.

(23) Thompson, M. W. Energy spectrum of ejected atoms during high-energy sputtering of gold. *Philos. Mag.* **1968**, *18*, 377–414.

(24) Sigmund, P. Theory of sputtering. I. Sputtering yield of amorphous and polycrystalline targets. *Phys. Rev.* **1969**, *184*, 383–415.

(25) Riederer, D.E.; Chatterjee, R.; Rosencrance, S.W.; Postawa, Z.; Dunbar, T.D.; Allara, D.L.; Winograd, N. Thermal desorption induced by kiloelectronvolt ion bombardment

---

of thiol-bound self-assembled monolayers on gold. *J. Am. Chem. Soc.* **1997**, *119*, 8089-8094.

(26) Chatterjee, R.; Riederer, D. E.; Postawa, Z.; Winograd, N. Coverage-dependent molecular ejection from ion-bombarded C_6H_6/Ag{111}. *J. Phys. Chem. B* **1998**, *102*, 4176-4182.

(27) https://www.tec-science.com/thermodynamics/kinetic-theory-of-gases/maxwell-boltzmann-distribution/

(28) Garrison, B. J.; Delcorte, A.; Krantzman, K. D. Molecule liftoff from surfaces. *Acc. Chem. Res.* **2000**, 33, 70-77.

(29) Smiley, E. J.; Postawa, Z.; Wojciechowski, I.A.; Winograd, N.; Garrison, B.J. Coarse-grained molecular dynamics studies of cluster-bombarded benzene crystals. *Appl. Surf. Sci.* **2006**, 252, 6436-6439.

(30) Delcorte, A.; Garrison, B.J. Sputtering Polymers with Buckminsterfullerene Projectiles: A Coarse-Grain Molecular Dynamics Study. *J. Phys. Chem. C.* **2007**, *111*, 15312–15324.

(31) Hamraoui, K.; Delcorte, A. Effects of molecular orientation and size in sputtering of model organic crystals. *J. Phys. Chem. C* **2010**, 114, 5458–5467.

(32) Delcorte, A.; Bertrand, P. Kinetic energy distributions of secondary molecular ions from thin organic films under ion bombardment. *Nucl. Instrum. Methods Phys. Res. B* **1996**, *115*, 246-250.

(33) Delcorte, A.; Bertrand, P. Energy distributions of hydrocarbon secondary ions from thin organic films under keV ion bombardment: correlation between kinetic and formation energy of the ions sputtered from tricosenoic acid. *Nucl. Instrum. Methods Phys. Res. B* **1996**, *117*, 235-242.

(34) Seah, M.P.; Havelund, R.; Gilmore, I.S. Universal equation for argon cluster size-dependence of secondary ion spectra in SIMS of organic materials. *J. Phys. Chem. C* **2014**, *118*, 12862−12872.

(35) Czerwinski, B.; Delcorte, A. Molecular dynamics study of fullerite cross-linking under keV C_{60} and Ar_n cluster bombardment. *J. Phys Chem. C* **2013**, *117*, 3595−3604.

(36) Delcorte, A.; Garrison, B.J.; Hamraoui, K. Dynamics of molecular impacts on soft materials: from fullerenes to organic nanodrops. *Anal. Chem.* **2009**, *81*, 6676–6686

(37) Seah, M. P. Universal equation for argon gas cluster sputtering yields. *J. Phys. Chem. C* **2013**, *117*, 12622−12632.

---

(38) Delcorte, A.; Bertrand, P. Sputtering of parent-like ions from large organic adsorbates on metals under keV ion bombardment. *Surf. Sci.* **1998**, *412/413*, 97–124.

(39) Schueler, B.; Beavis, R.; Ens, W.; Main, D.E.; Tang, X.; Standing, K. G. Unimolecular decay measurements of secondary ions from organic molecules by time-of-flight mass spectrometry. *Int. J. Mass Spectrom. Ion Proc.* **1989**, *92*, 185–194.

(40) Gillen, G. The use of kinetic energy distributions to determine the relative contributions of gas-phase and surface fragmentation in kiloelectronvolt ion sputtering of a quaternary ammonium salt. *Int. J. Mass Spectrom. Ion Proc.* **1991**, *105*, 215–224.

(41) Delcorte, A.; Bertrand, P. Metastable decay of molecular fragment ions sputtered from hydrocarbon polymers under keV ion bombardment. *Int. J. Mass Spectrom. Ion Proc.* **1999**, *184*, 217-231.

(42) Delcorte, A.; Garrison, B. J. Desorption of large molecules with light-element clusters: Effects of cluster size and substrate nature. *Nucl. Instrum. Methods Phys. Res. B* **2011**, *269*, 1572–1577.

(43) Mücksch, Ch.; Anders, Ch.; Gnaser, H.; Urbassek, H. M. Dynamics of L‑phenylalanine sputtering by argon cluster bombardment. *J. Phys. Chem. C* **2014**, *118*, 7962−7970.

(44) Czerwinski, B.; Rzeznik, L.; Paruch, R.; Garrison, B. J.; Postawa, Z. Effect of impact angle and projectile size on sputtering efficiency of solid benzene investigated by molecular dynamics simulations. *Nucl. Instrum. Methods Phys. Res. B* **2011**, *269*, 1578-1581.

(45) Postawa, Z.; Paruch, R.; Rzeznik, L.; Garrison, B.J. Dynamics of large Ar cluster bombardment of organic solids. *Surf. Interface Anal.* **2013**, *45*, 35–38.

(46) Delcorte, A. Organic surfaces excited by low-energy ions: atomic collisions, molecular desorption and buckminsterfullerenes. *Phys. Chem. Chem. Phys.* **2005**, *7*, 3395-3406.

(47) Sheraz née Rabbani, S.; Berrueta Razo, I.; Kohn, T.; Lockyer, N. P.; Vickerman, J. C. Enhancing ion yields in time-of-flight-secondary ion mass spectrometry: a comparative study of argon and water cluster primary beams. *Anal. Chem.* **2015**, *87*, 2367−2374.

(48) Delcorte, A.; Moshkunov, K.; Debongnie, M. Relationships between crater and sputtered material characteristics in large gas cluster sputtering of polymers: Results from molecular dynamics simulations. *J. Vacuum Sci. Technol. B*, **2018**, *36*, 03F109.

Figure 1. Intensity of the signal of Si^+ sputtered from a clean silicon wafer by 30-keV Bi_5^+ as a function of the reflector voltage of the TOF.SIMS 5 instrument (Integral KED). Dashed line: fit with the integral of a Sigmund-Thompson function. Full line: Sigmund-Thompson distribution derived from the fit.

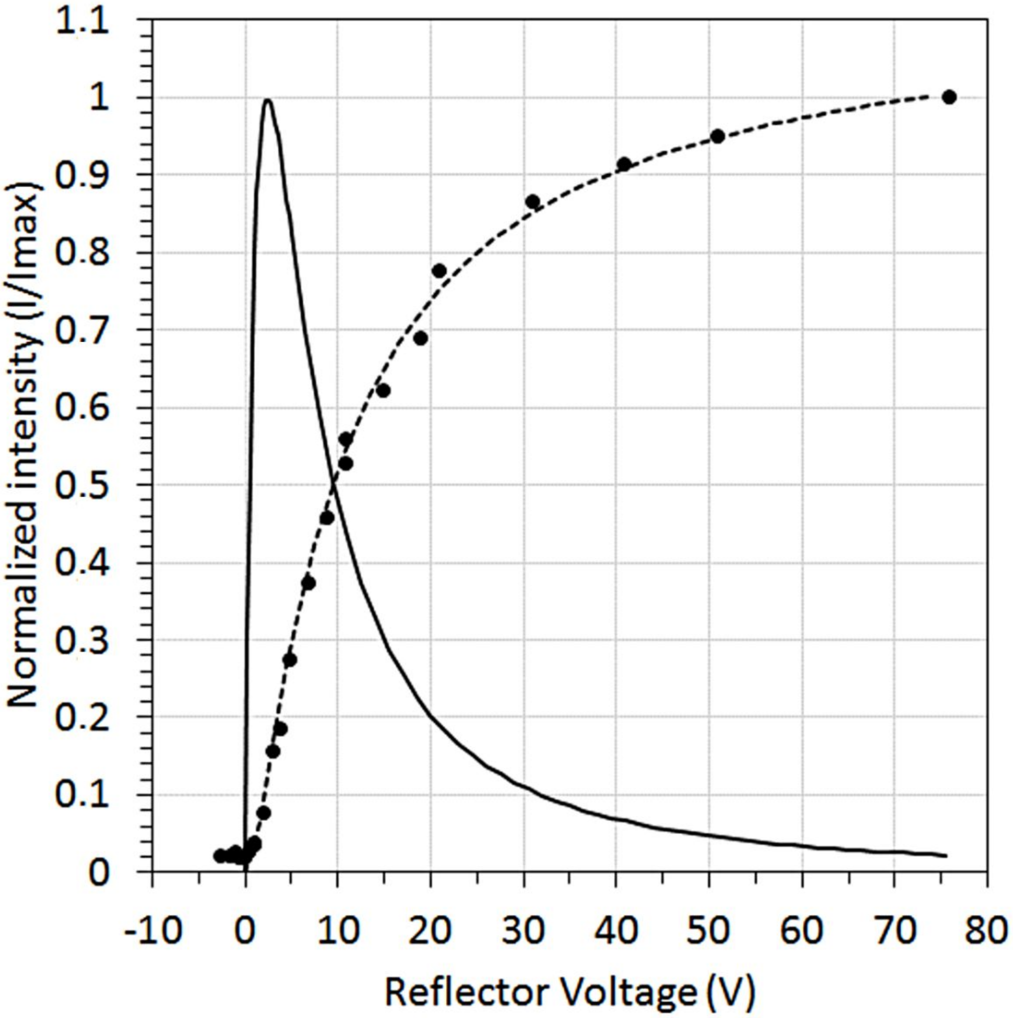

Figure 2. Maxwell-Boltzmann energy distributions derived from the fit of the integral KED of $C_xH_y^+$ ions sputtered from Irganox 1010 under 30 keV Bi_5^+ bombardment

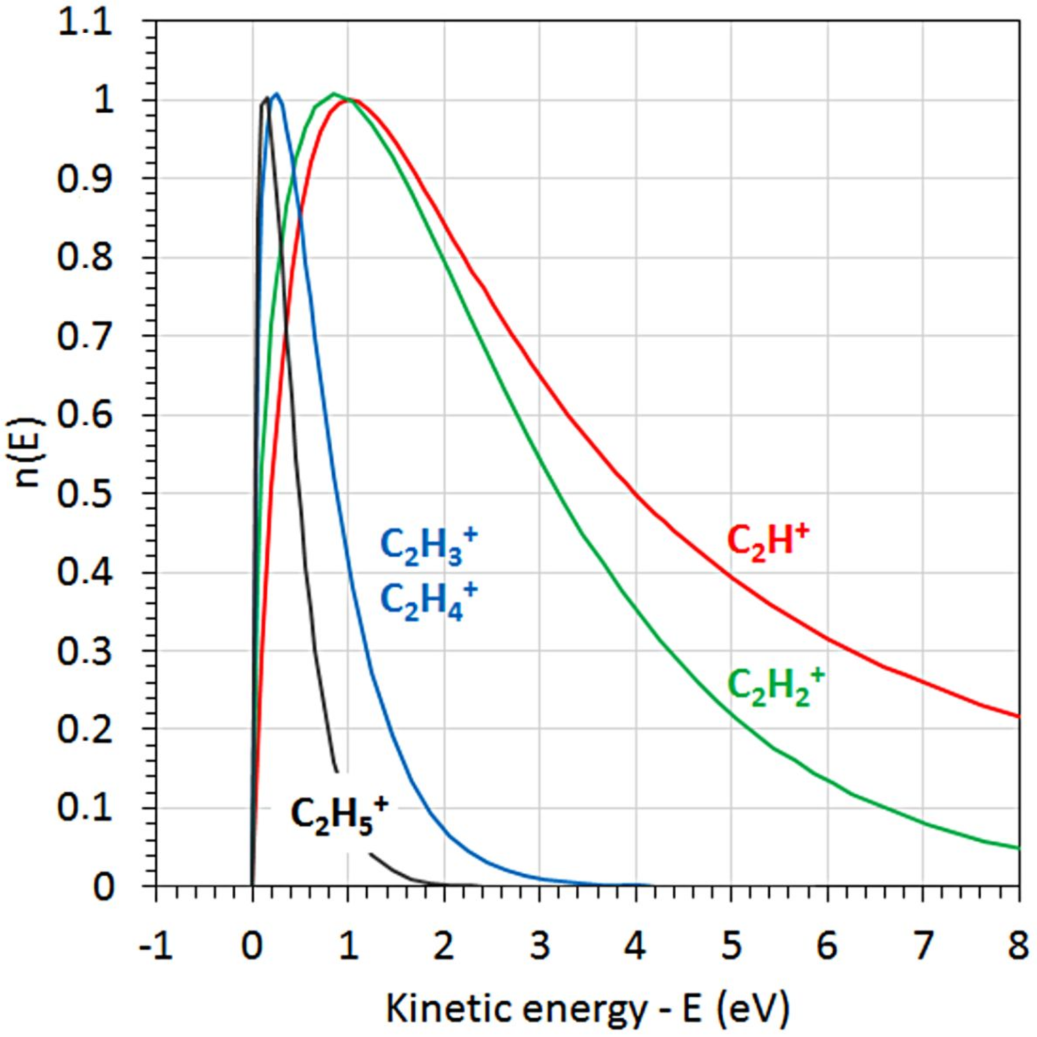

Figure 3. (a) Normalized intensities of the signals of (M-H)$^-$ sputtered from Irganox 1010 by various cluster projectiles, as a function of the reflector voltage of the TOF.SIMS 5 instrument (Integral KED). *Lines:* Fits of the data with the integrals of Maxwell-Boltzmann functions. (b) Maxwell-Boltzmann energy distributions derived from the fit of the integral KEDs of (a).

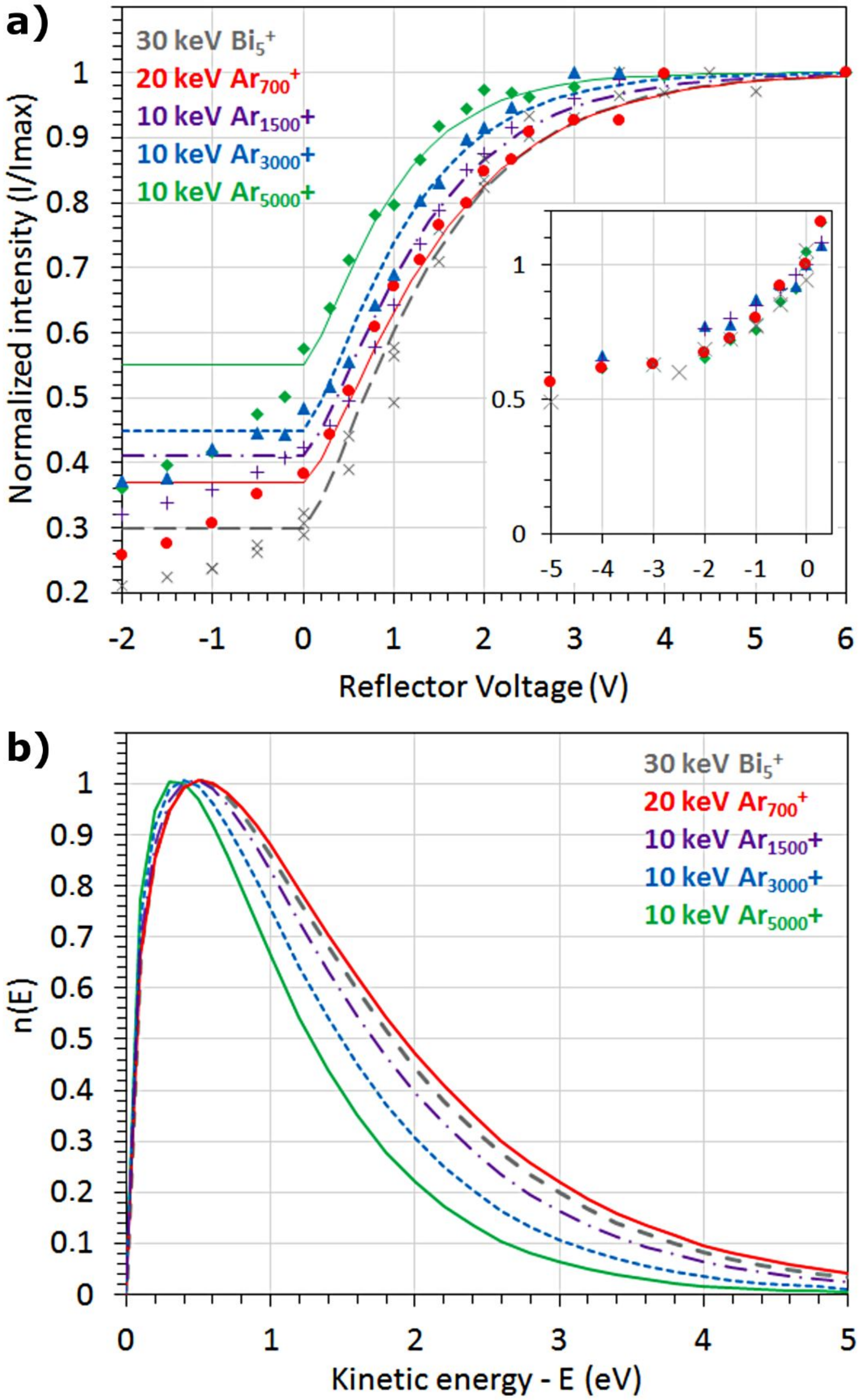

Figure 4. (a) FWHM of the axial KEDs of (M-H)$^-$ sputtered from Irganox 1010 by 30 keV Mn$^+$, Bi$^+$, Bi$_5^+$ and by a series of Ar$_n^+$ cluster projectiles, as a function of the scaled energy *E/n*. (b) Fraction of (M-H)$^-$ ions formed in the gas phase. *Error bars:* estimated ±0.05 eV uncertainty on the data and fits.

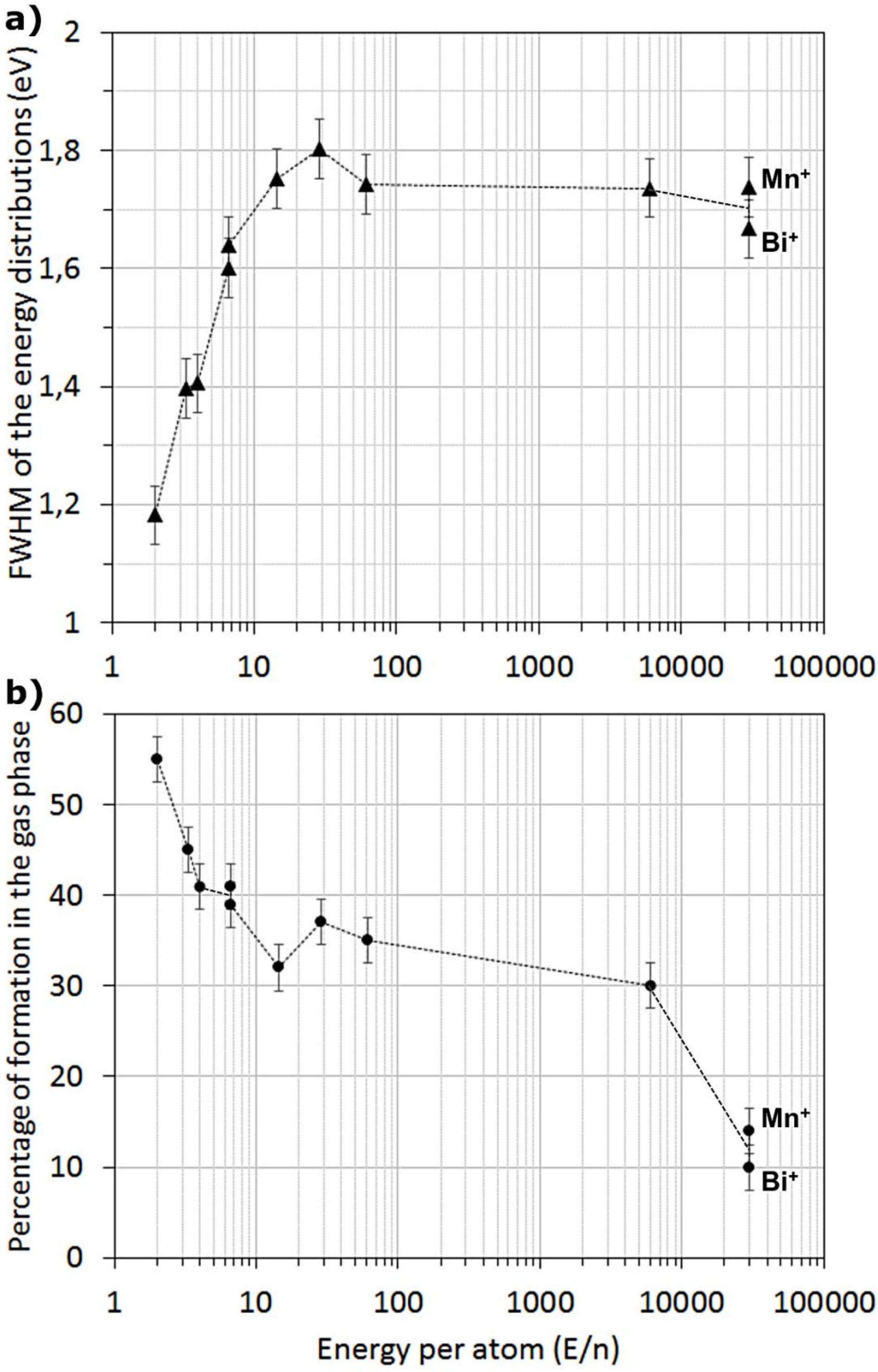

Figure 5. Normalized intensity of the signal of (M-H)$^-$ (black) and dimers (2M-H)$^-$ (red) sputtered from Irganox 1010 as a function of the reflector voltage of the ION.TOF 5 instrument (Integral KED). *Dashed lines:* fit with the integral of Maxwell-Boltzmann distribution functions. *Full lines:* Maxwell-Boltzmann distributions derived from the fit.

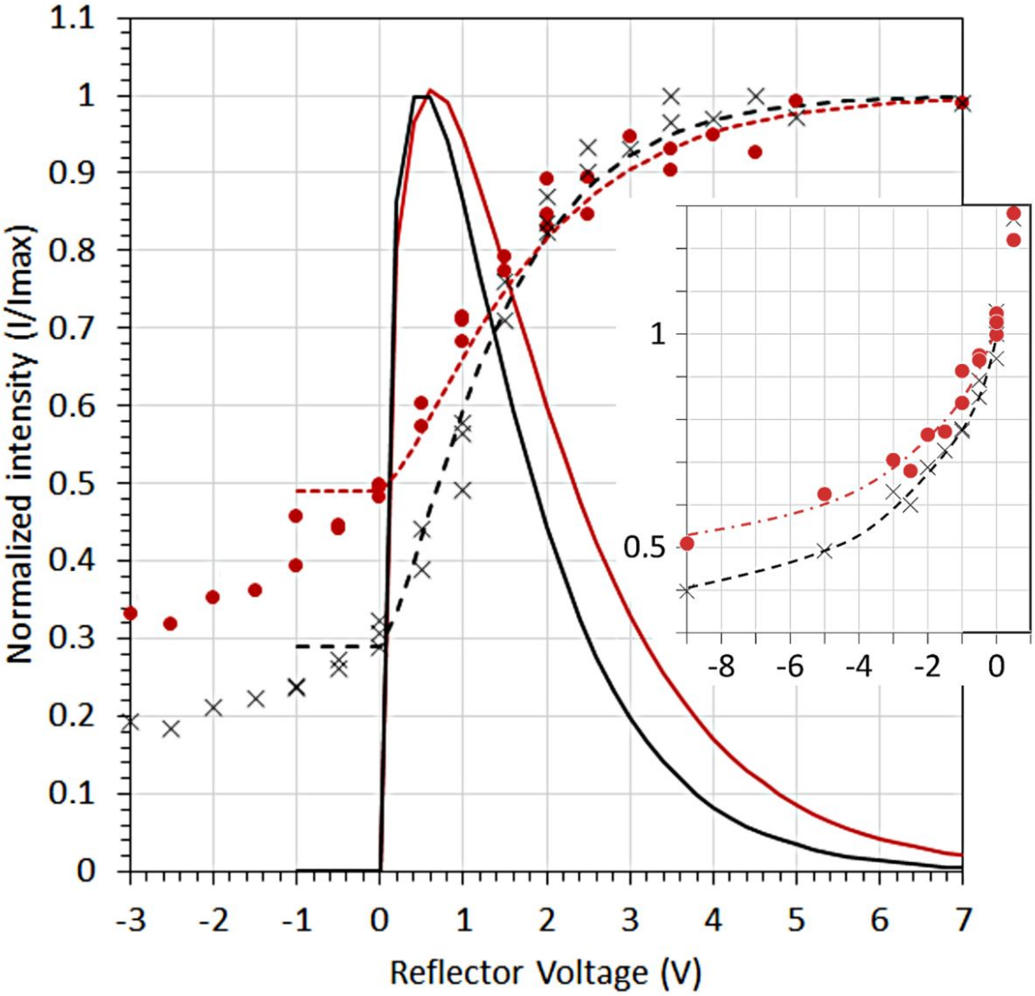

Figure 6. Normalized intensities of the signals of the molecular ion $M^{\cdot+}$ and fragments H^+, CH_3^+ and $[CH_2\text{-}(C_6H_2)\text{-}(C_4H_9)_2\text{-}OH]^+$ sputtered from Irganox 1010 by (a) 30 keV Bi_5^+ and (b) 10 keV Ar_{3000}^+ cluster bombardment, as a function of the reflector voltage of the ION.TOF 5 instrument (Integral KED). *Lines:* Fits of the data with the integral of Maxwell-Boltzmann functions.

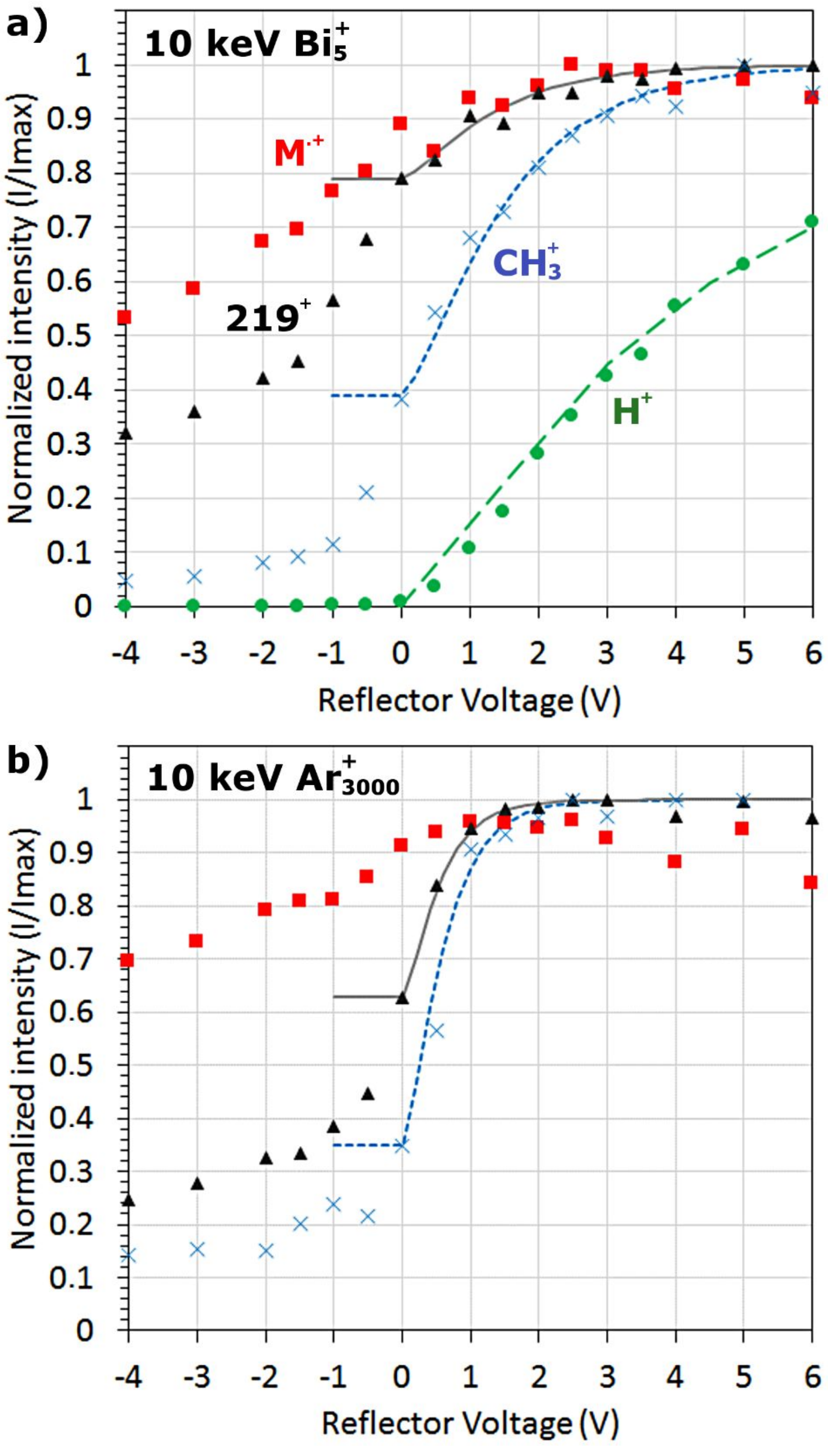

Figure 7. MD simulations of icosane bombarded by Ar_n clusters. (a) Average axial kinetic energies of the sputtered icosane molecules as a function of the scaled energy *E/n*. (b) Average total kinetic energies of the sputtered molecules. (c) Average emission angle (with respect to the sample normal). *Color coding:* black crosses – Ar_{5000}; green diamonds – Ar_{3000}; red triangles – Ar_{1000}; orange circles – Ar_{500}; blue crosses – Ar_{250}; open black circles – Ar_{60}; violet squares – Ar_{18}. The grey circles point to the two bombardment conditions used as examples in Fig. 8.

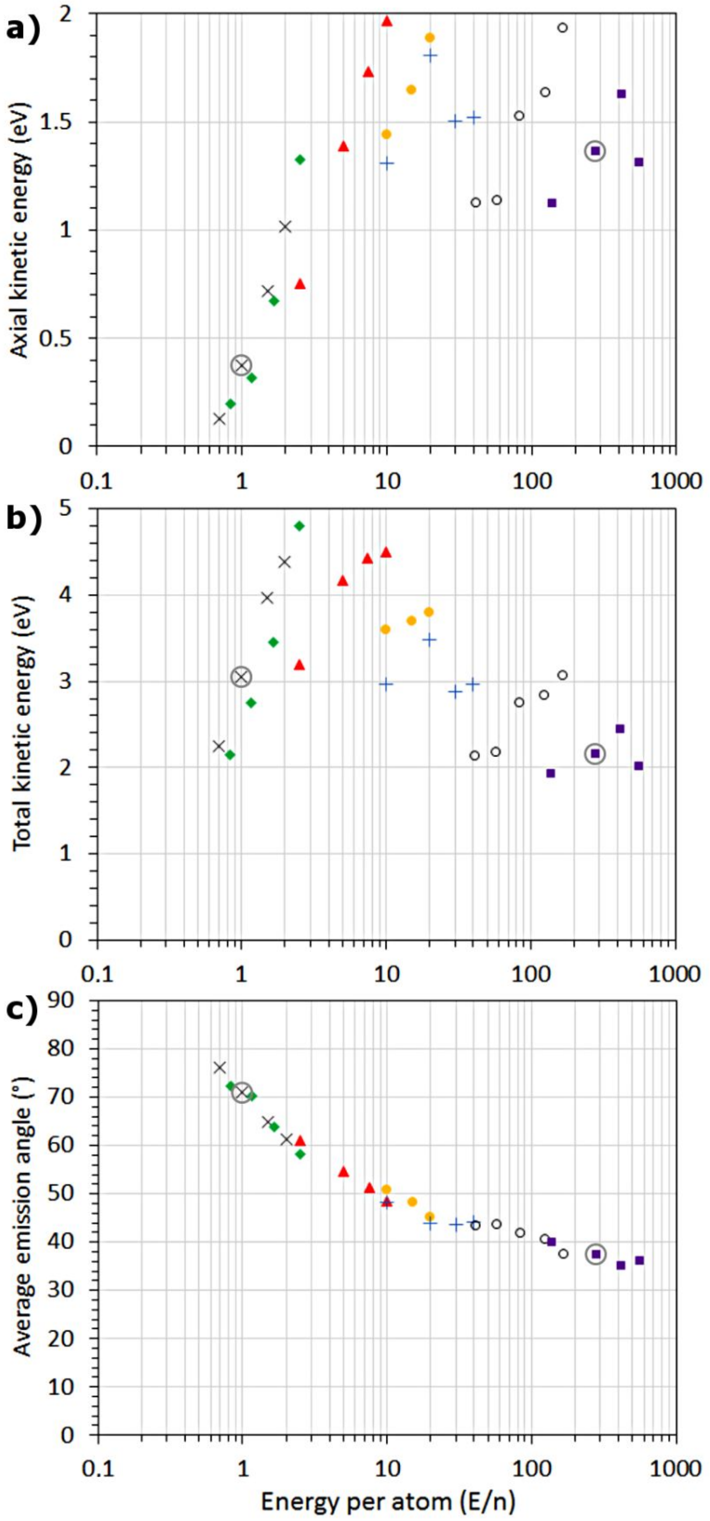

Figure 8. (a-d) Time evolution of the molecular dynamics. Side views of the icosane sample at different times of the sputtering event. Two bombardment conditions are superimposed for direct comparison, see grey circles in Fig. 7: 5 keV Ar_{18} – 278 eV/atom (projectile in green, icosane target in red), and 5 keV Ar_{5000} – 1 eV/atom (projectile in yellow, icosane target in blue). (a) 0 ps; (b) 5 ps; (c) 10 ps; (d) 20 ps. (e) Two measures of the velocity of the pressure waves propagating in the icosane solid: forward (*x* direction), full circles, and downward (*z* direction), crosses. The red triangles represent the ratio of the projectile over pressure wave forward (*x*) velocities.

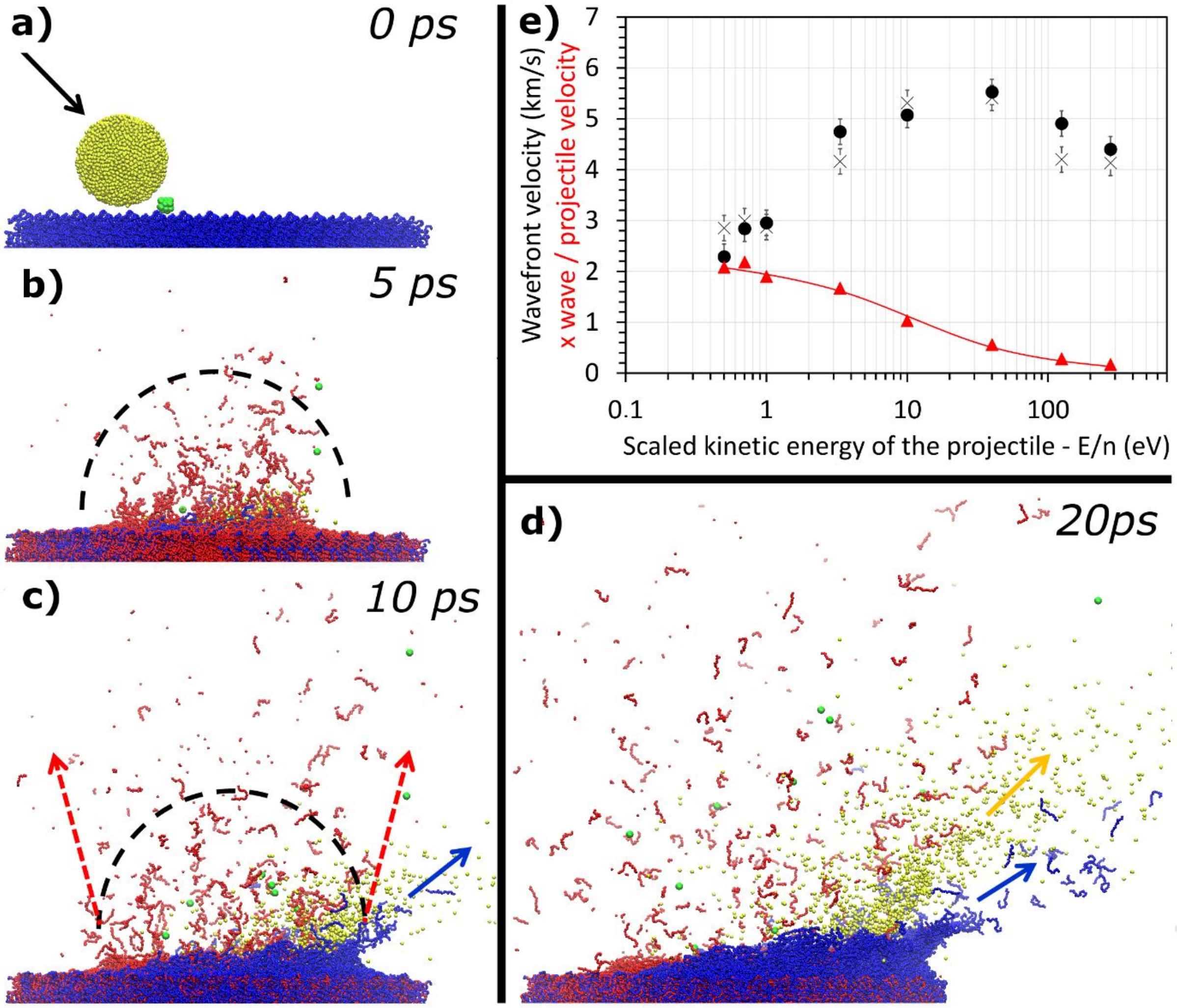

TOC graphic

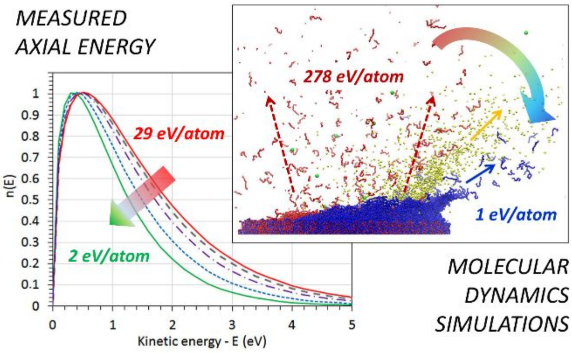
MEASURED
AXIAL ENERGY
29 eV/atom
2 eV/atom
n(E)
1
0.9
0.8
0.7
0.6
0.5
0.4
0.3
0.2
0.1
0
0
1
2
3
4
5
Kinetic energy - E (eV)
278 eV/atom
1 eV/atom
MOLECULAR
DYNAMICS
SIMULATIONS